Biomedical Optics

Photonic Crystal Fiber-Based Evanescent-Wave Sensor for Detection of Biomolecules in Aqueous Solutions

Jesper B. Jensen, Lars H. Pedersen, Poul E. Hoiby, Lars B. Nielsen, Theis P. Hansen, Jacob R. Folkenberg, Jesper Riishede, Danny Noordegraaf, Kristian Nielsen, Anneline Carlsen and Anders Bjarklev

We demonstrate[1] highly efficient evanescent-wave detection of fluorophore-labeled biomolecules in submicroliter aqueous samples positioned in the microstructured part of a photonic crystal fiber (PCF).[2] The airholes of the PCF provide access for the sample to regions with a strong optical field; this is in contrast to what occurs in the case of standard optical fibers, for which the coating and cladding must be removed to obtain an overlap between the optical field and the sample. PCF-based evanescent-wave sensors can therefore maintain both cladding and coating, which serves to ensure a robust device. A micrograph of the PCF used in our experiment is depicted in Fig. 1(a). Airholes with an average diameter of 3.4 μm are arranged in a triangular lattice with a 4-μm pitch. As illustrated in Fig. 1(b), the cladding crystal resembles a large number of air-suspended index-guiding core-like structures connected by thin silica bridges. Given the size of these structures, there is a strong penetration of the evanescent optical field—including for wavelengths in the visible range —into the sample. The fraction γ of the optical field intensity that propagates in the aqueous sample positioned in the airholes is calculated by use of a freely available full-vectorial plane-wave method.[3] For light with a free-space wavelength of $\lambda^* = 650$ nm, we determined that $\gamma = 5.2$ percent.

The reduced overlap between the optical fields and the sample in the PCF must be taken into account in any comparison between the PCF-based evanescent-wave sensor and a standard cuvette-based technique. One can achieve this comparison by scaling the interaction length with the intensity of the evanescent field, which corresponds to introducing an effective interaction length with 100 percent overlap between the light and the sample. With $\gamma = 5.2$ percent, the effective length of a 20-cm-long piece of the section equals 1.04 cm. Given the fiber dimensions, 20-cm fiber holds a sample volume of only 0.6 μl. Long effective interaction lengths can hence be achieved by use of small sample volumes. This is one of the advantages of using a PCF-based sensor in comparison with standard cuvette measurements.

The functionality of the PCF-based evanescent-wave sensor was illustrated by detecting Cy5-labeled DNA molecules in aqueous solutions. The airholes were filled with samples either by use of capillary force or by applying pressure to the sample. We derived the absorbance spectrum of the sample by comparing the transmission spectrum of the sample-filled PCF with that of a PCF that contained a reference. Figure 1(c) shows the transmission spectra of two 20-cm-long pieces of the PCF filled completely with a 5-μM Cy5-labeled DNA Oligo solution and pure water, respectively. The absorbance spectrum derived from these transmission spectra is shown in Fig. 1(d). It matches the absorbance spectrum of the Cy5 molecule, thus confirming that the sample contains the Cy5-labeled DNA.

In conclusion, PCF-based evanescent-wave sensors can be used to detect labeled biomolecules in submicroliter sample volumes, an important application in, for example, biotechnological production of hybrid probes.

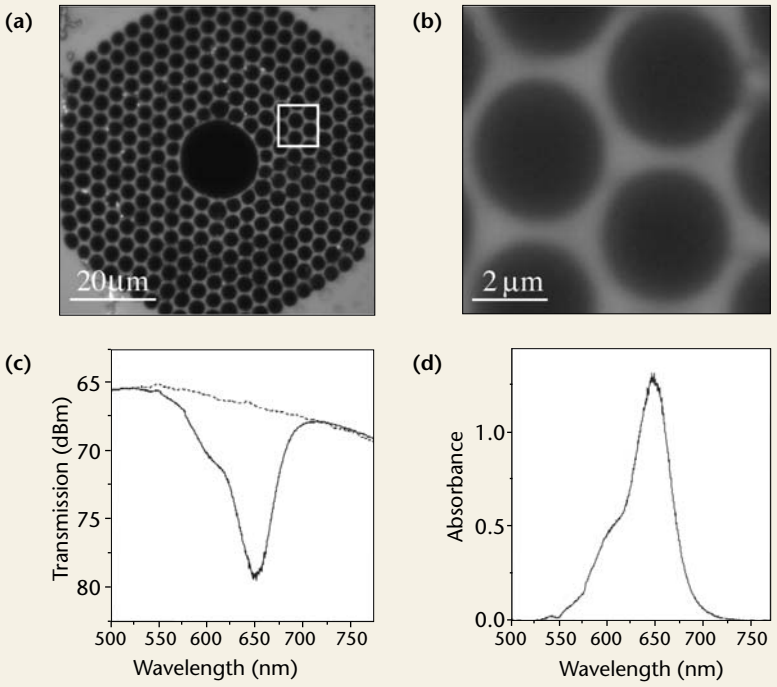

Figure 1. (a) Micrograph of the microstructured part of the PCF. (b) Close-up of the framed section in (a), showing the air-suspended core-like structures in the cladding crystal. (c) Transmission spectra of two PCFs with a 5-μM Cy5-DNA solution (solid line) and a pure water reference (dashed line), respectively. (d) The derived absorbance in the sample that contains the Cy5-labeled DNA solution, showing the characteristic Cy5 absorbance spectrum.

Jesper B. Jensen (jbj@com.dtu.dk), Jesper Riishede, Danny Noordegraaf, Kristian Nielsen, Anneline Carlsen and Anders Bjarklev are with Research Center COM, Technical University of Denmark, Lyngby, Denmark. Lars H. Pedersen, Poul E. Hoiby and Lars B. Nielsen are with Bioneer A/S, Hørsholm, Denmark. Theis P. Hansen is with Research Center COM, Technical University of Denmark, Lyngby, Denmark and Crystal Fibre A/S, Birkerød, Denmark. Jacob R. Folkenberg is with Crystal Fibre A/S, Birkerød, Denmark.

References

1. J. B. Jensen et al., Opt. Lett. **29**, 1974–6 (2004).
2. J. C. Knight et al., Opt. Lett. **21**, 1547–9 (1996).
3. S. G. Johnson and J. D. Joannopoulos, Opt. Express **8**, 173–90 (2001), http://www.opticsexpress.org.

Complex Fourier Domain Optical Coherence Tomography Using the Heterodyne Technique

Jun Zhang and Zhongping Chen

Optical coherence tomography (OCT) is a noninvasive, noncontact imaging modality which uses coherent gating to obtain high-resolution cross-sectional images of tissue microstructure.[1] Fourier domain OCT (FDOCT) has attracted much attention recently in comparison with conventional time domain OCT (TDOCT) because of its potential for higher sensitivity and higher imaging speed.[2] In addition to the morphological structural image, FDOCT can also provide functional information on tissue physiology. In TDOCT systems, a phase-resolved approach has been shown to be an effective method for the high speed acquisition of functional information on tissue characteristics such as blood flow velocity and birefringence.[3] The same approach can be used in FDOCT systems to reconstruct intensity and functional images by processing the complex signals from the sample. However, the imaging range of FDOCT is limited by the mirror image that accompanies the structural image as a result of Fourier transform. What's more, in FDOCT, the reflected terms from the reference mirror and sample always yield DC noise and low frequency autocorrelation noise. These parasitic terms obscure the structure of the object and generate phase error, which compromises the reconstruction of complex fringe signals.

Our recent work shows how use of a heterodyne technique can generate a full-range complex signal in FDOCT thanks to the complete elimination of DC noise, autocorrelation noise and mirror images.[4] By choice of an appropriate carrier frequency generated by an electro-optic (EO) phase modulator in our swept source based FDOCT system, the positive and negative frequency terms of the Fourier transformed interference fringe signal can be separated from each other and from the low frequency noise. In this way, the complex signal containing both the amplitude and phase terms can be reconstructed by selection of the positive (or negative) frequency term. From the amplitude term of the complex signal, the structural image can be acquired. Figures 1(a) and 1(b) show the imaging of a rabbit cornea by means of the conventional FDOCT system and our novel FDOCT system, respectively. With our FDOCT system and the heterodyne technique, the imaging range was doubled thanks to cancellation of the overlapped mirror images. In addition, the elimination of the autocorrelation noise close to the zero position increased the signal to noise ratio by 20 dB. To illustrate the performance of our system in the acquisition of functional information, tissue birefringence was imaged by processing the phase and amplitude terms. Figure 1(c) shows the phase retardation image of a rabbit tendon. The intensity and birefringence images demonstrated the ability of our system to acquire structural and functional information on biological tissue. In summary, we presented, to the best of our knowledge for the first time, use of the heterodyne technique in FDOCT for the reconstruction of the complex fringe interference term. The technique has the potential for ultrahigh speed and ultrahigh resolution functional FDOCT in biomedical imaging.

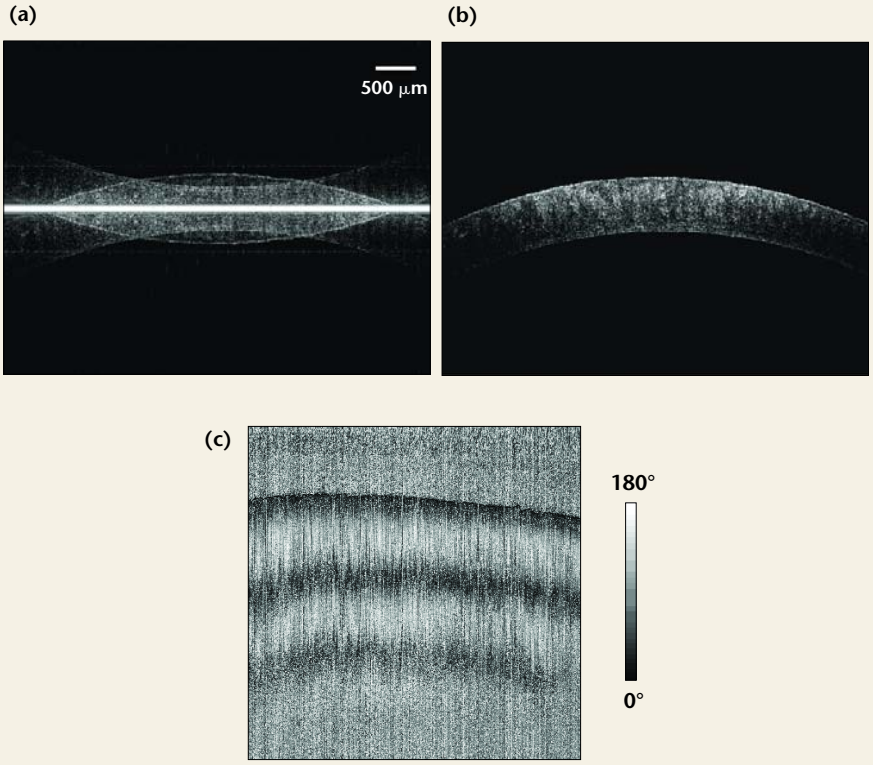

Figure 1. (a) Image of rabbit cornea acquired by conventional FDOCT system. (b) Image of rabbit cornea acquired by means of complex FDOCT system which uses the heterodyne technique. (c) Phase retardation image of rabbit tendon using the complex FDOCT system.

Jun Zhang (junzhang@uci.edu) and Zhongping Chen (zchen@bli.uci.edu) are with the Beckman Laser Institute and the Center for Biomedical Engineering, University of California, Irvine.

References

1. D. Huang, et. al., Science **254**, 1178-81 (1991).
2. R. Leitgeb, et. al., Opt. Express **11**, 889-94 (2003).
3. H. Ren, et. al., Opt. Lett. **27**, 1702-4 (2002).
4. J. Zhang, et. al., "Removal of mirror image and enhancement of signal to noise ratio in Fourier domain optical coherence tomography using an electro-optic phase modulator." Opt. Lett.

A Combined Corneal Topographer & Aberrometer Based on Shack-Hartmann Wave-Front Sensing

Fan Zhou, Xin Hong, Donald T. Miller, Arthur Bradley and Larry N. Thibos

Monochromatic aberrations of the eye degrade retinal image quality and lead to poor visual performance. Therefore whole-eye aberrometry based on Shack-Hartmann wave-front sensing (SHWS) technology can provide a powerful means to predict the optical performance of the eye[1]. The performance of the cornea alone, however, is not revealed by whole-eye aberrometry, the results of which are determined by the interaction of the cornea and lens. Understanding the cornea's optical role is critical because it contributes the majority of the total refractive power of the eye and its optical quality can be compromised by ocular pathologies (keratoconus) and ophthalmic corrections (contact lenses, orthokeratology and refractive surgeries).

Placido-ring corneal topography is routinely used to assess the shape and inferred aberrations of the anterior cornea, the most important optical surface of the eye. However, measurement inaccuracies, arc-step assumptions, approximations in the reconstruction algorithm and potential skew ray errors all limit the accuracy of such instruments, particularly for non-radially-symmetric corneas.[2] We have developed and validated a new type of corneal topographer based on SHWS which overcomes many of the limitations of Placido topographers and allows noninvasive measurement of both the shape and the aberrations of the cornea. Because most components of our instrument are the same as those used for whole-eye aberrometry, our new topographer can be easily combined into a single instrument to quickly meausre corneal topography and whole-eye aberrometry.[3] The instrument schematics and a typical example of the measured results from our combined instrument are illustrated in Fig. 1. When the device is used as a whole-eye aberrometer, a narrow laser beam is focused by the eye onto one point on the subject's retina. Reflected light from this point source emerges from the eye to be sampled at 400 μm intervals by a microlenslet array and recorded with a CCD camera. From this information, a refractive wave aberration map is computed. To measure corneal aberrations with this instrument, a custom low-aberration high-numerical-aperture (NA) lens is strategically positioned in front of the eye with its focal point at the nominal center of curvature of the cornea. The reflective wave front from the cornea is spatially resolved with a sampling density of 130 μm. Novel algorithms were developed to obtain the corneal topography and refractive aberrations from the measured reflective aberrations. In our beta version of the combined instrument, corneal and whole-eye aberrometry can be obtained by switching in and out the high-NA objective in front of the cornea.

Measurements of reflective aberrations on calibrated model corneal surfaces correlated well with theoretical predictions ($R^2 = 0.964$ to 0.994). The root-mean-square corneal sag error was small for the reconstructed corneal surface, ranging from 0.1 to 0.17 μm for four of five model corneas with a range of asphericities and radii comparable to those of human corneas. The corneal refractive aberrations derived from the measured reflective aberrations matched—within a small fraction of a wavelength—theoretical predictions and the empirical refractive aberrometry data obtained from each model. The measurement repeatability on human corneas was < 1 μm for the corneal topography and < 1/9 λ (λ = 0.633 μm) for the higher-order refractive aberrations.

The technical advantage of this instrument has been used to address fundamental clinical questions.[4,5] These studies illustrate the instrument's potential application in clinical diagnostics and in scientific research in the field of corneal optics.

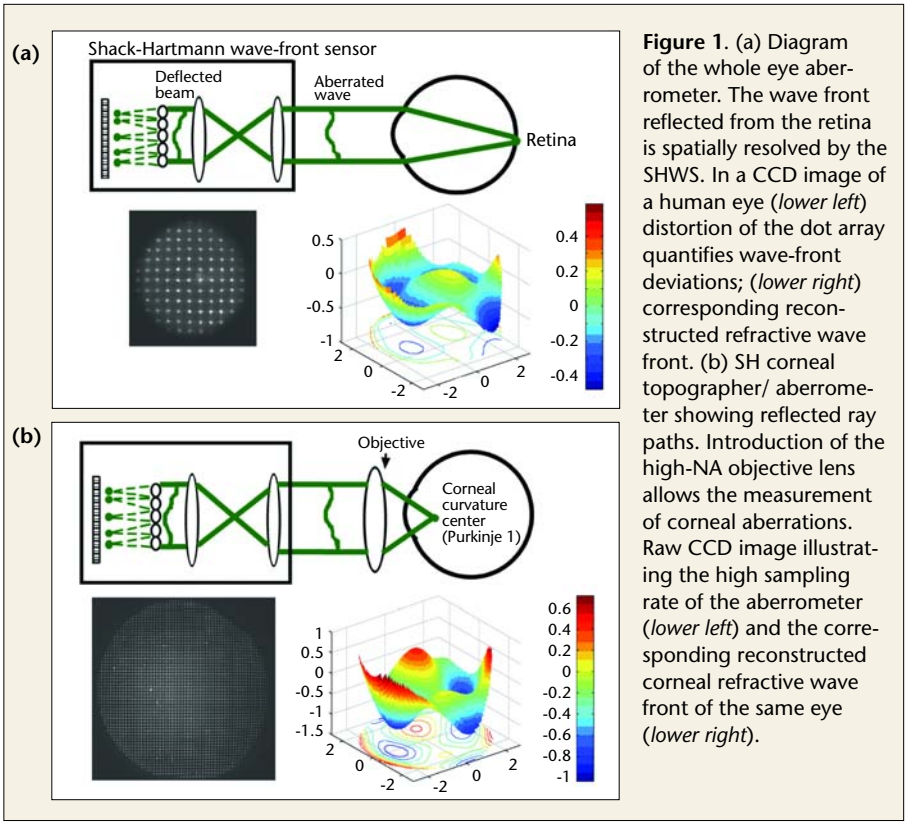

Figure 1. (a) Diagram of the whole eye aberrometer. The wave front reflected from the retina is spatially resolved by the SHWS. In a CCD image of a human eye (*lower left*) distortion of the dot array quantifies wave-front deviations; (*lower right*) corresponding reconstructed refractive wave front. (b) SH corneal topographer/ aberrometer showing reflected ray paths. Introduction of the high-NA objective lens allows the measurement of corneal aberrations. Raw CCD image illustrating the high sampling rate of the aberrometer (*lower left*) and the corresponding reconstructed corneal refractive wave front of the same eye (*lower right*).

Fan Zhou (fanoliviazhou@hotmail.com), Xin Hong, Donald T. Miller, Arthur Bradley and Larry N. Thibos are with the School of Optometry, Indiana University, Bloomington.

References

1. L. N. Thibos et al., J. Opt. Soc. Am. A Opt. Image Sci. Vis. **19**, 2329-48 (2002).
2. R. A. Applegate et al., Optom. Vis. Sci. **72**, 785-92 (1995).
3. F. Zhou et al., J. Opt. Soc. Am. A Opt. Image Sci. Vis. **21**, 683-6 (2004).
4. F. Zhou et al., Invest Ophthalmol. Vis. Sci. **45**, ARVO E-Abstract 2833 (2004).
5. F. Zhou et al., Optom. Vis. Sci. **80**, S3 (2003).